STUDY ON DENSIFICATION OF IRON-TIN GRADED MATERIAL OBTAINED BY SELECTIVE LASER MELTING

Cleiton André Comelli, cleiton.comelli@gmail.com[1]
Luiza Bertoldo Benedetti, luizabenedetti@gmail.com[1]
Carlos Henrique Ahrens, carlos.ahrens@ufsc.br[1]

[1]Universidade Federal de Santa Catarina, R. Eng. Agronômico Andrei Cristian Ferreira, s/n - Trindade, Florianópolis - SC, 88040-900.

Abstract. *The manufacturing of functionally graded materials (FGM) is based on structural or compositional variation through the part. A possible technology to obtain such materials is selective laser melting (SLM), an additive manufacturing (AM) technique that offers flexibility in multiple processing parameters while processing different materials at once. One of the interest fields includes materials with different tribological and mechanical properties. In this study, cube specimens were manufactured with varied composition and process parameters, aiming to obtain optimized consolidation in each composition of a discrete gradient between pure iron up to iron with 25 wt. % of tin. Pure iron powder, iron powder with 12.5 wt. % of tin and iron powder with 25 wt. % of tin were used to obtain specimens. The energy density was varied within the composition by changing the scan spacing, laser power and scanning speed parameters. Following this methodology, it was possible to conclude that a higher energy application produce warpage, and a lower energy level results in very porous or even non-densified specimens. The results were analyzed using scanning electron microscopy (SEM) and response surface methodology (RSM), showing the variation of density in function of the process parameters applied.*

Keywords: *Functionally graded materials, Selective laser melting, Additive manufacturing, Iron, Tin.*

1. INTRODUCTION

FGM are part of an engineering materials class which exhibit heterogeneous properties due to variation in the structure or composition throughout the volume, resulting in optimized chemical, physical or geometric configurations (MIYAMOTO et al., 1999; RABIN; SHIOTA, 1995).

The mainly FGM manufacturing techniques includes powder metallurgy (PM), centrifugal casting (CS), vapor deposition techniques (VDT) and additive manufacturing (AM). AM is a new method to manufacture FGM and one of the most promising, thanks to its unique process features and characteristics (GUPTA; TALHA, 2015). The main advantage of this technology is the material layer stacking process, that shapes parts in a flexible way, allowing the creation of almost any geometry with no adding cost with increasing component complexity (GAO et al., 2015; VOLPATO et al., 2007).

The main AM techniques for FGM manufacturing are based on selective laser melting (SLM) or selective laser sintering (SLS) of powder layers. Kruth et al. (2007), report that when laser is used as an energy source to consolidate layers of powder material, the processing of a wide range of materials becomes possible, including ceramics, polymers, metals or composites. Also according to the author, the materials processed by SLS or SLM have several particle consolidation mechanisms, and the composition and final structure is dependent of process parameters and powder properties.

Table 1 presents the main SLS/SLM processing parameters, sorting them into two groups, the first related to the material and the second to the process (YADROITSEV; BERTRAND; SMUROV, 2007; KRUTH et al., 2005; CHILDS; HAUSER; BADROSSAMAY, 2004; SIMCHI, 2004; TAYLOR, 2002).

Table 1 – Parameters that influence the SLS / SLM process.

Parameters	
Related to material	Related to process
Chemical properties	Laser Power
Thermal properties	Laser wavelength
Optical properties	Laser beam diameter
Metallurgical properties	Laser scan speed
Mechanical properties	Scan spacing
Rheological properties	Layer thickness
Particle size distribution	Scan strategy
Particle shape	Energy density

The control of parameters variation contribute to the use of additive manufacturing to produce FGM, as confirmed by various studies exploring several applications.

BEAL (2005), used SLM to produce a gradient between tool steel and copper, starting from 100 wt. % tool steel to a concentration of 50 wt. % copper and 50 wt. % tool steel. He looked for improvements in thermal conduction for specific regions of an injection mold.

MUMTAZ; HOPKINSON (2007), using the same process, obtained a FGM between Waspaloy and Zirconia, starting from 100 wt. % Waspaloy up to 90 wt. % Waspaloy and 10 wt. % Zirconia. An improvement in zirconia adhesion in Waspaloy was found by using a gradient between the two materials, therefore reducing residual stresses .

MAHAMOOD; AKINLABI (2015), using the laser metal deposition (LMD) technique, produced a gradient of Ti6Al4V and TiC, starting from 0 wt. % TiC to 50 wt. % TiC and 50 wt. % of Ti6Al4V. The results showed that optimized parameters for each composition of the gradient produced better results of hardness and wear resistence.

FGM can also be used to improve composite materials exposed to vibration, friction and mechanical stress, since regions with abrupt transitions tend to generate residual stresses which are reduced by the gradual transition promoted by FGM (JUNG et al., 1997). Furthermore, stress concentration at the interface between directly jointed materials (DJM) promotes crack formation, responsible for failures in some bearing components (LEADER, 2001) or heat Shields (COOLEY, 2005;KOIZUMI; NIINO, 1995).

In this context, fabrication and testing of a FGM manufactured by SLM is explored. The objective is to evaluate the consolidation and understand the effects of material mixing and processing parameters in the results.

2. MATERIALS AND METHODS

3.1. Feedstock powders

To investigate the influences of the process parameters in the manufacture of a FGM, two particulate materials were used as feedstock, one composed of iron (Höganäs AHC 100.29) and the other of eutectic Sn-Ag alloy (Heraeus). Table 2 present the feedstock properties.

Table 2 – Feedstock powders.

Powder	Type of atomization	Particle size distribution (µm)	Particle morphology	Bulk density (g/cm^3)
Höganäs AHC 100.29	Water	20 a 200	Irregular (sponge-like)	2.95
Heraeus Sn 96.5 Ag 3.5	Gas	15 a 25	rounded	4.25

The chemical composition for both materials was evaluated (Figure 1) by energy-dispersive x-ray spectroscopy (EDX). The EDX analysis was performed in a JEOL JSM-6390LV machine with 15.0 kV of accelerating voltage.

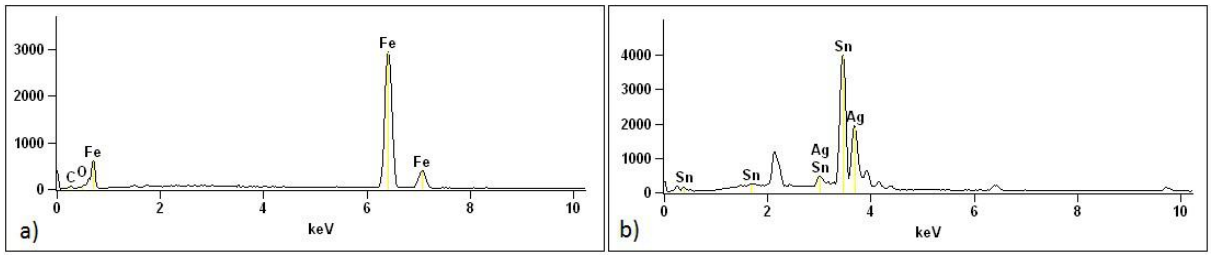

Figure 1 – EDX of feedstock powders: a) Iron powder b) Tin Powder.

Iron powder was composed of approximately 99.56 wt. % of iron with some oxygen (0.44 wt. %). The measured composition for tin powder was 95.83 wt. % Sn and 4.17 wt. % Ag.

Figures 2A and 2B were obtained by scanning electron microscopy (SEM) and show the morphology of the powders used. In the image B it is possible to see the spherical powders particles of tin powder, assigned to the gas atomizing in which the material has undergone. Image A shows the irregular shape of iron powder, more compatible with the water atomization technique used in its fabrication.

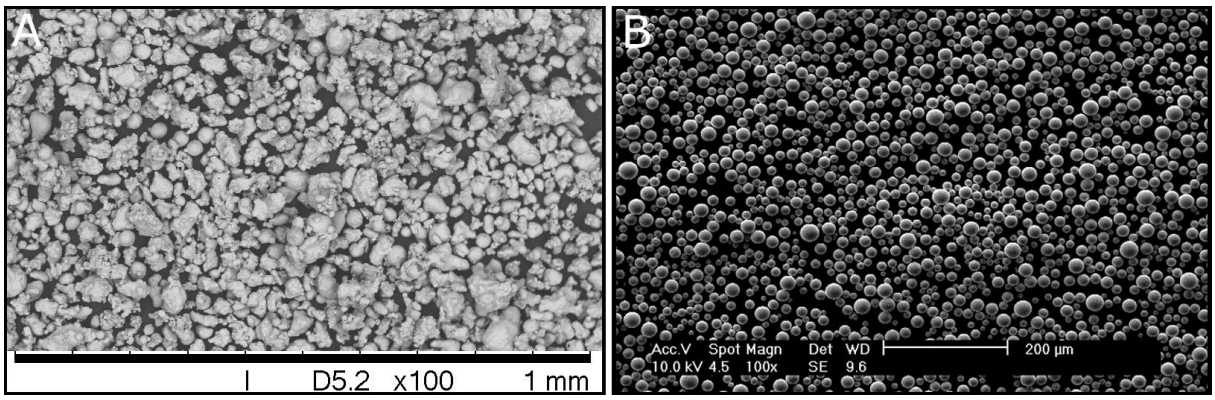

Figure 2 - A) Iron powder B) Tin powder.

2.2. Powder preparation for FGM compositions

Stock tin powder was used while iron powder was sieved at 106 µm to provide a better control of size distribution. Three different compositions were prepared with the two feedstock powder and named L, M and H:

•Pure iron powder (L composition);
•Iron powder with 12.5 wt. % of tin powder (M composition);
•Iron powder with 25 wt. % of tin powder (H composition).

Each material prepared represents a single step of the FGM material. The maximum amount of tin powder mixed to iron was set at 25 wt. %, since larger quantities restricted the flowability of the powder, required by the spread mechanism of the SLS/SLM machine available.

The mixtures were prepared with a Y mixer and the characterization was made with a CILAS 1190 particle size analyzer and hall funnel (MPIF Standard 04).

2.3. SLS/SLM machine

For processing the materials a prototype SLS/SLM machine was used. The machine was developed by Alkimat company, headquartered in Florianópolis/SC in partnership with the NIMMA laboratory. The main SLS/SLM machine components are:

•A 100 W laser source
•A galvanometer mirror module
•An elevation drive system
•An automated powder deposition

The atmosphere was monitored by an O_2 sensor and the levels were controlled with argon circulation during the entire process.

The chamber was made of acrylic and a glass window was used to allow the laser beam to reach the building substrate. The thickness of each deposited layer was controlled by the base downwards movement in relation to the powder dispenser device.

Each new layer is deposited using a mobile funnel. Figure 3 shows schematically the conception and parts of the equipment.

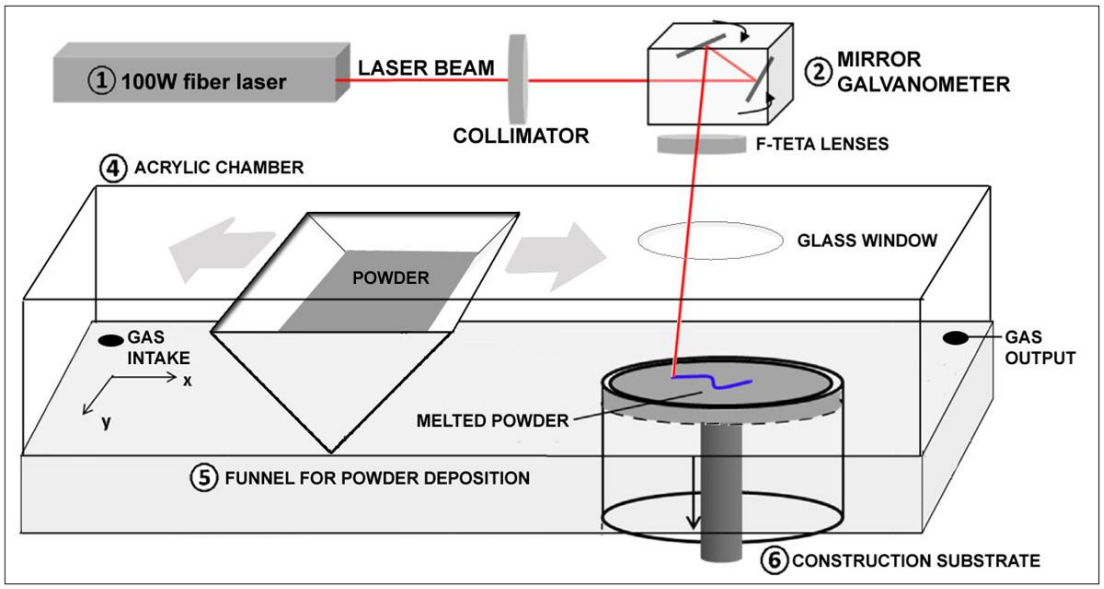

Figure 3 - Simplified scheme of the SLS/SLM device used.

2.4. Specimens fabrication and evaluation

The specimens were built in two steps. Initially, a process window was defined; the limits were obtained by checking the minimum and maximum energy density for each composition in a single layer experiment. In the condition of maximum power density, the layers produced should not suffer warpage or distortion, while in the minimum energy condition; a satisfactory sintering of particles should be achieved.

In the second step, a response surface method (RSM) experiment was used to find optimal processing parameters for each composition. Box-Behnken methodology was applied to set a response surface mesh and find the ideal processing point for each composition of the material. The main goal of the experiment was to maximize consolidation.

Samples of 10x10x7 mm were produced, 15 for each composition; all experiments were repeated 3 times, totaling 45 samples for each composition. The parameters controlled during the manufacturing were power, scan speed and hatching distance. These variables are part of energy density equation, which is given by

$$\varphi = \frac{P}{u \times h \times D} \tag{1}$$

where φ is the energy density (J/mm3), P is the laser power (W), u is the scan speed (mm/s), h is the scan spacing (hatching) (mm) and D is the thickness of the powder layer (mm).

The density of each sample produced was measured using a caliper and an analytical balance (M-214 Bel-AI). For the statistical analysis Statgraphics software was used. The surface of the specimens was evaluated by scanning electron microscopy (SEM).

3. RESULTS AND DISCUSSION

3.1. Characterization of gradient compositions

The particle size analysis shows the percentiles for 10, 50 and 90%, besides the average particle diameter of each powder prepared. The bulk density and flow time were also measured.

The results of the particle size characterization of each prepared powder are presented by Table 3.

Table 3 - Results of the characterization of the three compositions studied.

Property	Fe<106 µm	87.5% Fe 12.5% Tin	75% Fe 25% Tin
Percentile 10%	30.86 µm	26.65 µm	19.83 µm
Percentile 50%	68.95 µm	70.88 µm	58.80 µm
Percentile 90%	114.81 µm	120.05 µm	109.60 µm
Average diameter	71.48 µm	73.11 µm	61.84 µm

Table 4 shows the density measured for each composition.

Table 4 – Bulk density of the three compositions studied.

Composition		M (g) (25 cc)					m(g) Avg	ρ (g/cm^3)	Std dev
Iron	**<106**	75.20	74.41	74.49	74.46	74.61	74.63	2.99	0.32
87.5% Fe+12.5% Tin	**<106**	79.60	78.67	78.83	78.52	78.89	78.90	3.16	0.42
75% Fe 25% Tin	**<106**	87.64	89.57	87.99	89.42	87.55	88.43	3.54	0.98
50 % Fe 50% Tin	**<106**	101.49	99.22	100.66	100.57	102.23	100.83	4.03	1.13

It is possible to observe an increasing bulk density with the increase of tin added to the mixture; this can be attributed to the difference in particle size between the powders. The smaller particles of tin powder fit between the larger particles of iron powder, filling the voids and increasing the bulk density. This characteristic is beneficial for the process, as greater values of bulk density make it easier to consolidate the particles with laser.

Table 5 shows the flowtime measured for each composition prepared.

Table 5 - Flowability of the three compositions studied.

Powder		T(s)					T(s) Avg	Std dev
Iron	**<106**	25.90	25.15	24.16	24.60	24.23	24.81	0.73
87.5% Fe+12.5% Sn-Ag	**<106**	20.85	20.61	20.44	20.82	20.73	20.69	0.17
75% Fe 25% Sn-Ag	**<106**	16.36	16.71	16.43	16.63	16.89	16.60	0.21
50 % Fe 50% Sn-Ag	**<106**	*	*	*	*	*	*	*

*Lack of flowability

Even with the increase in bulk density, a decrease of flow time was observed with the addition of tin powder, this could be attributed to the tribological characteristics of tin, which may have actuated in order to reduce the friction among particles. However, for higher amounts of tin, it was observed a lack of powder flowability, which can be attributed to the high bulk density of the powder and a consequent packing of the particles.

3.2. Process window

In this experiment layers were produced and classified; the feasible parameters were obtained from the approved ones. To be approved, the layer must be well adhered to the substrate, with defined contours and good particles consolidation. Figure 4 shows some samples of layers produced and their classification.

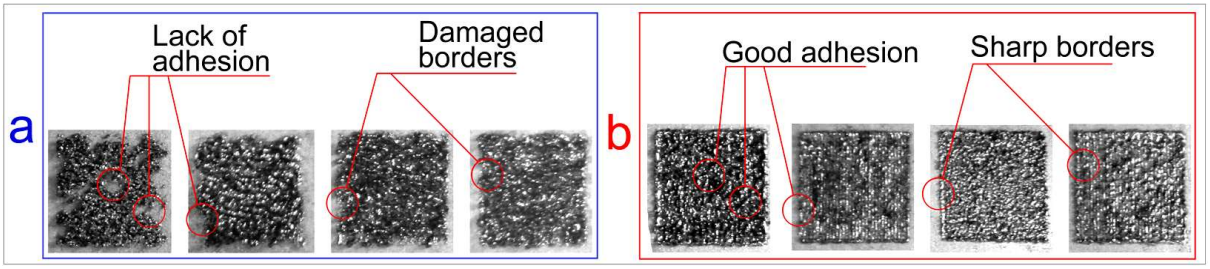

Figure 4 – Single layers produced: a) Reproved b) Approved.

During the single layer experiment it was observed that the powders prepared with tin required lower energy densities when compared to iron powder, which can be explained by the relative low melting point of this material if compared to iron.

Furthermore, the materials showed a higher sensitivity to laser scanning speed variations, when compared with power variations or distance between lines. Thus, in order to vary energy density, speed was the calibrated parameter for each composition. Table 6 shows the laser parameters and energy density range used.

Table 6 – Parameters range.

Composition	Scan speed		Laser power		Hatching		Energy density	
	Minimun	Maximum	Minimun	Maximum	Minimun	Maximum	Minimun	Maximum
	mm/s	mm/s	W	W	mm	mm	J/mm^3	J/mm^3
L	70	170	80	94	0.08	0.15	31.0	141.2
M	95	195	80	94	0.08	0.15	27.0	104.1
H	120	220	80	94	0.08	0.15	24.0	82.4

3.3. Parameters optimization

Samples were produced in order to define the processing parameters that optimize densification for each composition. To evaluate the effect of the parameters an experimental project was elaborated, varying power, scanning speed and hatching distance within the range obtained from single layers experiment.

After fabrication, the volumetric density of each specimen was measured, and the data was used to compare the effect of processing parameters in the measured density. Figures 5, 6 and 7 show the individual influence of parameters variation on density for each composition.

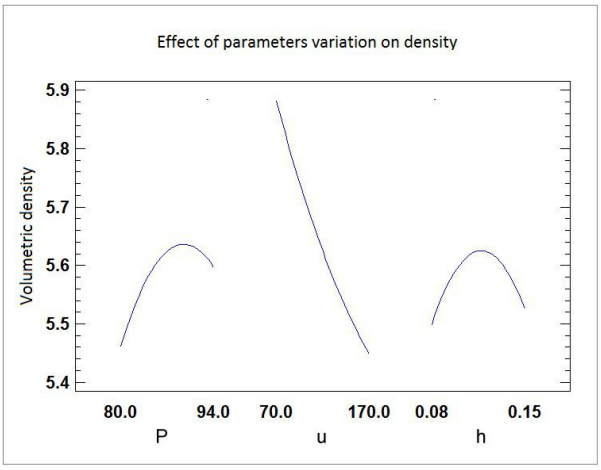

Figure 5 - individual influence of parameters variation on density for L composition.

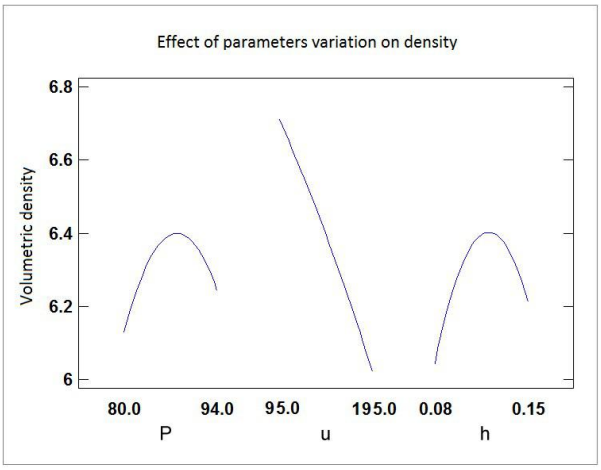

Figure 6 - individual influence of parameters variation on density for M composition.

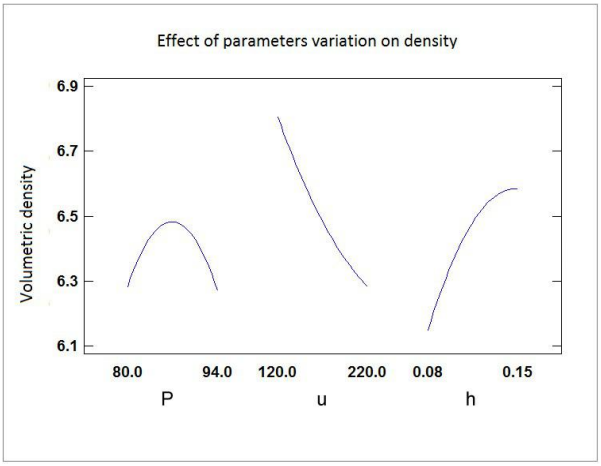

Figure 7 - individual influence of parameters variation on density for H composition.

It is possible to observe the distinctive effect of each parameter on density, and that speed variation has a bigger influence compared with power variation and hatching distance.

The increase in power and hatching distance raises density up to a limit value, which when exceeded, causes a decrease in density. For the power, it is possible to note that after the threshold value is exceeded, the minimum density attained, i.e. when the system operates at maximum power, is smaller as the amount of tin increases. Possibly such behavior can be assigned to a bigger melting in compositions with higher amounts of tin, generating instabilities in the molten pool and resulting in porous structures.

When hatching distance is analyzed, the opposite effect is observed; maximum values for hatching distances resulted in higher density values as tin concentration increases. This behavior possibly happens because this parameter acts lowering remelting and decreasing instability promoted by the low melting point of tin.

To provide a wide view of achievable densities, a response surface mesh was obtained. The axes represent the respective values for power (x-axis) velocity (y-axis) and hatching distance (z-axis). By varying the colors of each grid point, it is possible to check the combination of parameters to obtain a specific densification. Figure 8 shows the mesh obtained for composition L.

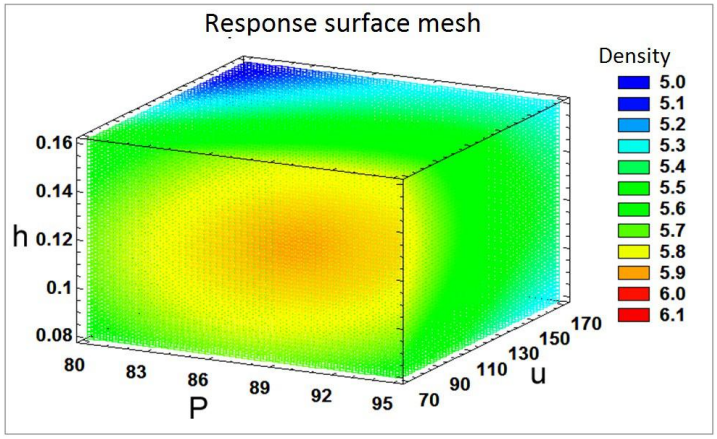

Figure 8 - Response surface mesh for composition L.

The parameters for maximum density obtained from the RSM are 90.3W for power, 70mm/s for scanning speed and 0.12 mm for hatching distance. The resulting energy density of this set of parameters is 97.6 J/mm^3.

The same procedure was repeated for composition M, the results are shown in Figure 9.

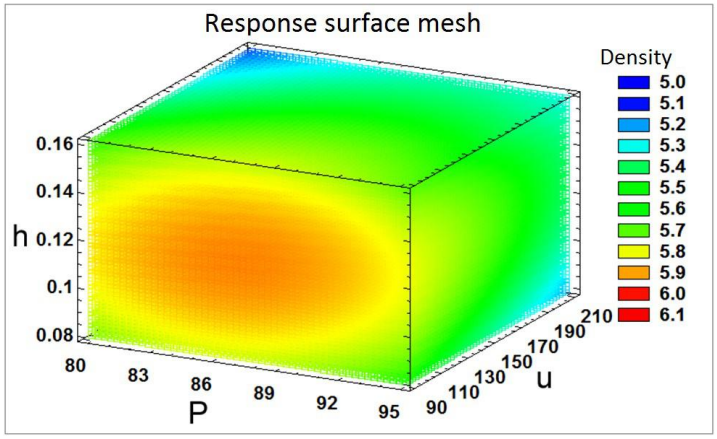

Figure 9 - Response surface mesh for composition M.

Compared to iron powder, the addition of 12.5% of tin moves the region with higher densities to the left. For this composition the optimized parameters for the highest density were 86.9 W for power, 95 mm/s for scanning speed and 0.12 mm for hatching distance. The resulting energy density of this set of parameters is 69.3 J/mm^3.

Figure 10 shows RSM for the H composition.

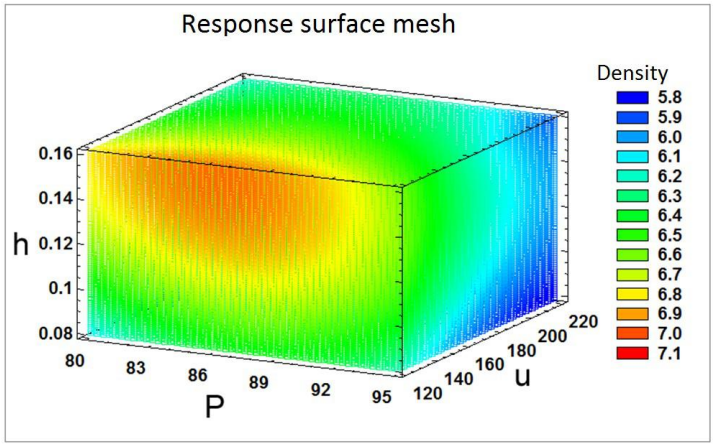

Figure 10 - Response surface mesh for H composition.

The parameters for maximum density of phase H are 86.3 W for power, 120 mm/s for scanning speed and 0.15 mm for hatching distance. The resulting energy density of this set of parameters is 43.6 J/mm^3.

The surface mesh showed a bigger shift of the red region to the negative direction of the x axis, that is, in the sense of lowering power. Respectively to this, the red region has shifted in the positive direction of z axis, showing that greater distance between the lines enhance the densification of the parts.

This behavior can be associated with the largest melting capacity of the particulate material, given the larger amount of Sn-Ag in the mixture. It is possible that with the increasing amount of tin powder, the diameter of the weld pool increases as well, allowing a good filling of processed area even with bigger hatching distances.

2.2. Analysis of the surface by SEM

After obtaining the optimized processing parameters for each of the compositions, new test samples were produced and the surface of each was analyzed by scanning electron microscopy (SEM). The pieces presented a relative consolidation of 71% for L composition, 85% for M composition and 89% for H composition.

Figure 11 shows the images obtained by SEM of the surface of each of the compositions, in order of increasing tin concentration.

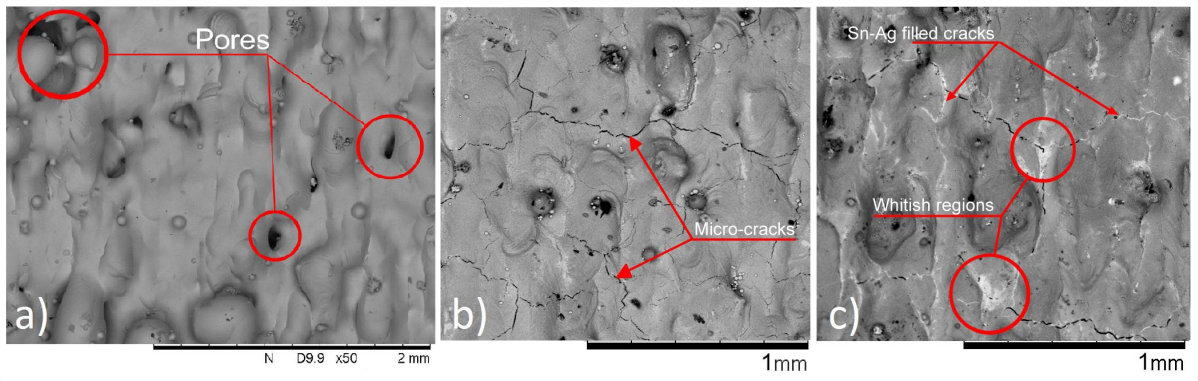

Figure 11 - Surface processed by SLM: a) Phase L b) Phase M c) Phase H.

The images show the presence of pores and cracks. It is possible to observe a high concentration of micro-cracks in phases containing tin and whitish regions in the phase with the highest concentration of tin. Also, laser scan lines aligned in the vertical direction of the images are visible for all compositions.

The presence of porosity can be explained by the irregular shape of the iron powder and the high average of particle size (80 µm) for processing by SLM. In addition, the equipment used did not have powder compression system for spreading powder layers; they were simply deposited by gravity, a factor that may have contributed to a minor consolidation.

The increased density observed with the addition of tin might also be better understood by analyzing the SEM images. It is possible to note that the tin reduces the number of large pores, though contribute to the appearance of micro-cracks in the material, probably by promoting a hardening and consequent weakening of the formed structure.

The images also indicate that with the increase of 12.5 wt.% to 25 wt.% of tin in the material composition, whitish regions and tin filled cracks emerge on surface, indicating a tin saturated mixture. This might have caused segregation regions and even promoted the filling of micro-cracks with tin as the second material to solidify.

2.2. Conclusions

The manufacture of specimens through the SLM process proved to be viable. It was concluded that the phases of the functional gradient material exhibited increases in density due to the addition of tin.

The achieved density values are relatively low by today's standards processing by SLM. However, this study was valid since it used two materials with very distinct melting points and properties not studied in the literature found of SLM process or FGM production.

Furthermore, the density values can be enhanced with the use of powders with spherical morphology and a spreading system capable of promoting a higher packing of the particles during the deposition of the layers. It is also possible to study the effect of potential additives that enhance iron wettability during processing. Changes in the manufacturing process, including pre-heating the building substrate and remelting each layer can also be applied.

SEM analysis of the materials showed the formation of micro-cracks in materials composed of tin and iron, showing a greater fragility promoted by the addition of this element in the resulting structure. Such weakness can be explained by internal tensions generated by interactions between the elements and the rapid melting and solidification in which the process expose the processed materials.

It should also be taking into account that tin has tetragonal crystal structure, different from iron which has crystalline body-centered cubic structure, a factor that can distort the resulting crystal structure, increasing the hardness but also the brittleness. Additionally, the large difference between the melting points creates regions rich in tin, formed in segregated regions with later solidification.

4. ACKNOWLEDGEMENTS

The authors would like to thank the Federal University of Santa Catarina, the NIMMA laboratory, the department of Mechanical Engineering for the necessary support to carry out this work and CNPq for granting financial support.

5. REFERENCES

BEAL, V. E. FABRICATION OF FUNCTIONAL GRADIENTS BETWEEN TOOL STEEL AND COPPER PARTS BY SELECTIVE LASER FUSION USING A HIGH POWER Nd:YAG PULSED LASER BEAM TO INJECTION MOULDS APPLICATIONS. Florianópolis: Universidade Federal de Santa Catarina, 2005.
BHARTI, I.; GUPTA, N.; GUPTA, K. M. Novel applications of functionally graded nano, optoelectronic and thermoelectric materials. International Journal of Materials, Mechanics and Manufacturing, v. 1, n. 3, p. 221–224, 2013.
BRANCH, S. Laser synthesis of functional graded filter elements. Samara: [s.n.].
CHILDS, T. H. C.; HAUSER, C.; BADROSSAMAY, M. Mapping and Modelling Single Scan Track Formation in Direct Metal Selective Laser Melting. CIRP Annals - Manufacturing Technology, v. 53, n. 1, p. 191–194, 2004.
CHUNG, H.; DAS, S. Functionally graded Nylon-11/silica nanocomposites produced by selective laser sintering. Materials Science and Engineering A, v. 487, n. 1–2, p. 251–257, jul. 2008.
CLIMENTE, A.; TORRENT, D.; SÁNCHEZ-DEHESA, J. Gradient index lenses for flexural waves based on thickness variations. Applied Physics Letters, v. 105, n. 6, p. 64101, 2014.
COOLEY, W. G. Application of functionally graded materials in aircraft structures. 2005.
D. L. BOURELL, H. L. MARCUS, J. W. BARLOW, J. J. B. AND C. R. D. Multiple material systems for selective beam sinteringUnited States, 1991.
DECKARD, J. J. B. AND C. R. Selective laser sintering with assisted powder handlingUnited States, 1990.
GAO, W. et al. The status, challenges, and future of additive manufacturing in engineering. CAD Computer Aided Design, v. 69, p. 65–89, 2015.
GUPTA, A.; TALHA, M. Recent development in modeling and analysis of functionally graded materials and structures. Progress in Aerospace Sciences, p. 1–14, 2015.
JUNG, Y.-G. et al. Residual stress and thermal properties of zirconia / metal (nickel , stainless steel 304) functionally graded materials fabricated by hot pressing. Journal of Materials Science, v. 32, p. 3841–3850, 1997.
KOIZUMI, M.; NIINO, M. Overview of FGM Research in Japan. MRS Bulletin, v. 20, n. 1, p. 19–21, 1995.
KRUTH, J. P. et al. Consolidation phenomena in laser and powder-bed based layered manufacturing. CIRP Annals - Manufacturing Technology, v. 56, n. 2, p. 730–759, 2007.
KRUTH, J.-P. et al. Binding mechanisms in selective laser sintering and selective laser melting. Rapid Prototyping Journal, v. 11, n. 1, p. 26–36, 2005.
LEADER, M. Understanding Journal Bearings. Vibration Institute, Annual Meeting, 2001.
MAHAMOOD, R. M.; AKINLABI, E. T. Laser metal deposition of functionally graded Ti6Al4V/TiC. Materials & Design, v. 84, p. 402–410, 2015.
MISHINA, H.; INUMARU, Y.; KAITOKU, K. Fabrication of ZrO2/AISI316L functionally graded materials for joint prostheses. Materials Science and Engineering A, v. 475, n. 1–2, p. 141–147, 2008.
MIYAMOTO, Y. et al. Functionally Graded Materials Design, Processing and Applications. 1. ed. New York: Springer US, 1999.
MUMTAZ, K. A.; HOPKINSON, N. Laser melting functionally graded composition of Waspaloy and Zirconia powders. Journal of Materials Science, v. 42, n. 18, p. 7647–7656, 2007.
PATRI K. VENUVINOD, W. M. Rapid Prototyping Laser-based and Other Technologies. [s.l.] Springer Science & Business Media, 2004.
PEYRE, P. et al. Experimental and numerical analysis of the selective laser sintering (SLS) of PA12 and PEKK semi-crystalline polymers. Journal of Materials Processing Technology, v. 225, p. 326–336, 2015.
RABIN, B. H.; SHIOTA, I. Functionally Gradient Materials. MRS Bulletin, v. 20, n. 1, p. 14–18, 1995.
SHISHKOVSKY, I. Synthesis of functional gradient parts via RP methods. Rapid Prototyping Journal, v. 7, n. 4, p. 207–211, 2001.
SIMCHI, A. The role of particle size on the laser sintering of iron powder. Metallurgical and Materials Transactions B, v. 35, n. 5, p. 937–948, 2004.
TAYLOR, C. Morphology of direct SLS-processed stainless steel layers. Proceedings of Solid …, v. 44, n. 0, p. 530–537, 2002.
VOLPATO, N. et al. PROTOTIPAGEM RÁPIDA - TECNOLOGIAS E APLICAÇÕES. 1. ed. São Paulo: Blucher, 2007.
WONG, K. V.; HERNANDEZ, A. A Review of Additive Manufacturing. ISRN Mechanical Engineering, v. 2012, p. 1–10, 2012.
YADROITSEV, I.; BERTRAND, P.; SMUROV, I. Parametric analysis of the selective laser melting process. Applied Surface Science, v. 253, n. 19, p. 8064–8069, 2007.

6. RESPONSIBILITY NOTICE

The authors are the only responsible for the printed material included in this paper.